



Original Article

The effect of the number of subintervals upon the quantification of the seismic probabilistic safety assessment of a nuclear power plant

Ji Suk Kim, Man Cheol Kim*

Department of Energy Systems Engineering, Chung-Ang University, 84 Heukseok-ro, Dongjak-gu, Seoul, 06974, South Korea

ARTICLE INFO

Article history:

Received 23 September 2022

Received in revised form

14 December 2022

Accepted 25 December 2022

Available online 27 December 2022

Keywords:

Seismic probabilistic safety assessment

Seismic risk

Discrete approach

Discretization

Ground motion level intervals

Risk underestimation

Risk overestimation

ABSTRACT

Seismic risk has received increased attention since the 2011 Fukushima accident in Japan. The seismic risk of a nuclear power plant is evaluated via seismic probabilistic safety assessment (PSA), for which several methods are available. Recently, the discrete approach has become widely used. This approximates the seismic risk by discretizing the ground motion level interval into a small number of subintervals with the expectation of providing a conservative result. The present study examines the effect of the number of subintervals upon the results of seismic risk quantification. It is demonstrated that a small number of subintervals may lead to either an underestimation or overestimation of the seismic risk depending on the ground motion level. The present paper also provides a method for finding the boundaries between overestimation and underestimation regions, and illustrates the effect of the number of subintervals upon the seismic risk evaluation with an example. By providing a method for determining the effect of a small number of subintervals upon the results of seismic risk quantification, the present study will assist seismic PSA analysts to determine the appropriate number of subintervals and to better understand seismic risk quantification.

© 2022 Korean Nuclear Society, Published by Elsevier Korea LLC. This is an open access article under the CC BY-NC-ND license (<http://creativecommons.org/licenses/by-nc-nd/4.0/>).

1. Introduction

After seismic events such as the 2011 earthquake in Fukushima, Japan, the 2016 earthquake in Gyeongju, South Korea, and the 2017 earthquake in Pohang, South Korea, much attention has been focused on seismic risk [1–4]. Meanwhile, seismic probabilistic safety assessment (PSA) has gained much recognition for evaluating the safety of a nuclear power plant. Seismic PSA includes both hazard analysis and fragility analysis. Thus, the initiating event frequency can be determined by the hazard curve, which presents the annual exceedance frequency of the seismic event, while the failure probability of the system, structures, and components (SSCs) can be obtained from the fragility curve. The seismic PSA is quantified by calculating the convolutions of the hazard and fragility curves, and then evaluating the core damage frequency of a specific nuclear power plant due to a given seismic event.

Various quantification methods have been used in seismic PSA. For example, Kennedy [5] presented a closed form expression of the seismic risk for the entire ground motion level by assuming a hazard curve with a power-law distribution. However, it is difficult to obtain such closed-form expressions for most practical applications. While discrete probability distribution methods [6,7] have

been introduced, alternative quantification methods based on the Monte Carlo simulation and Latin hypercube sampling methods have been widely used. A hybrid method that combines sampling and discrete approaches was first proposed by Zhou et al. [8]. More recently, Watanabe et al. [9] developed a sampling approach for considering the correlations between failures; this approach was termed the direct quantification of a fault tree using the Monte Carlo simulation (DQFM). Subsequently, Kwag et al. [10,11] developed an improved DQFM method for quantifying the seismic risk with a smaller number of samples, and using Latin Hypercube sampling. However, an approach that uses discrete ground motion level subintervals has been most commonly used in recent years for the quantification of seismic PSA models [6,12,13]. In this approach, the ground motion level of interest is discretized into a small number of subintervals, the occurrence frequency for each subinterval is calculated from the hazard curve, and the corresponding failure probabilities of the SSCs are calculated from the fragility curve. This approach has the advantage of logically linking the primary seismic event tree and the secondary event trees that are used to further analyze the consequences of the primary event tree. This makes it possible to logically combine the failures in the primary and secondary event trees in minimal cut sets (unique combinations of component failures that can trigger system failure) and makes it easier and more convenient to evaluate these minimal cut sets. In addition, this approach makes it possible to build a multi-

* Corresponding author.

E-mail address: charleskim@cau.ac.kr (M.C. Kim).

unit risk assessment model by combining the seismic PSA models for multiple units.

However, while the accuracy of the approximation increases as the number of ground motion level subintervals increases, a small number of such subintervals (usually around five) is generally used to reduce the number of seismic PSA models that need to be handled. This is because a separate seismic PSA model is developed for each ground motion level subinterval. For example, the Risk Assessment of Operational Events Handbook [12] uses three ground motion level subintervals, while the Surry seismic PSA [14] uses eight. The use of such a small number of ground motion level subintervals has been accepted with the expectation that it will lead to conservative seismic risk quantification results.

The present study examines the effect of using a small number of ground motion level subintervals upon the results of seismic risk quantification. Specifically, the question of whether a small number of ground motion level subintervals will lead to an underestimation or overestimation of the seismic risk of a nuclear power plant is examined. Section 2 introduces the approach with discrete ground motion level subintervals, and analyzes the effect of the number of ground motion level subintervals upon seismic risk. Section 3 provides the method for identifying the ground motion level regions where the seismic risk may be underestimated when the number of ground motion level subintervals is small. Section 4 illustrates how a small number of ground motion level subintervals can lead to either an overestimation or underestimation of seismic risk. Section 5 provides a discussion of the results, and Section 6 summarizes the conclusions of the present study.

2. Seismic risk quantification using discrete ground motion level subintervals

2.1. Convolution of hazard and fragility curves

Theoretically, the seismic risk is quantified by the convolution of hazard and fragility curves according to Eq. (1) [5,7,15]:

$$P(x) = \int_0^{\infty} -\frac{dH(x)}{dx} F(x) dx \tag{1}$$

where $H(x)$ and $F(x)$ are the hazard and fragility curves for the ground motion level x . When the seismic risk is quantified for the ground motion level interval between a and b , the seismic risk can be approximated by the Riemann sum [16] as given by Eq. (2):

$$P(x) = \int_a^b -\frac{dH(x)}{dx} F(x) dx \approx \sum_{i=1}^N -h(x_i^*) F(x_i^*) \Delta x_i \tag{2}$$

where the ground motion level interval is discretized into N subintervals with x_0, \dots, x_N , and x_i^* 's are the midpoints for the Riemann sum; $h(x_i^*)$ is the first derivative of the hazard curve, and Δx_i is the width of the i -th subinterval (i.e., $\Delta x_i = x_i - x_{i-1}$). When each subinterval has an equal width, Δx_i is calculated by using Eq. (3):

$$\Delta x_i = \Delta x = \frac{b - a}{N} \tag{3}$$

The present study focuses on the case in which the subintervals are equally spaced, and the midpoints of subintervals are selected for the Riemann sum [16].

The hazard curve is generally a monotonically decreasing curve [17]. It describes the exceedance frequency of the seismic event versus peak ground acceleration. In the fragility curve, the failure

probability of an SSC increases curve as with the increase in ground motion level [18]. With reference to Kennedy [5,15], the hazard curve is assumed to be given by Eq. (4):

$$H(x) = K_I x^{-K_H} \tag{4}$$

where K_I is a constant, and K_H is the slope parameter.

Meanwhile, the fragility curve is given by Eq. (5):

$$F(x) = \Phi\left(\frac{\ln(x) - \ln(A_m)}{\beta_c}\right) \tag{5}$$

where $\Phi(\cdot)$ is the cumulative distribution function of a standard normal distribution, A_m is the median ground motion level capacity, and β_c is the composite variability. The latter is calculated by the root-sum-of-squares of the logarithmic standard deviations representing the random uncertainty (β_r) and the systematic or modeling uncertainty (β_u), i.e. $\beta_c = \sqrt{\beta_r^2 + \beta_u^2}$.

Finally, the integrand in Eq. (1) is defined as $G(x)$, and is given by Eq. (6):

$$G(x) = -h(x_i)F(x_i) = K_H K_I x^{-K_H-1} \Phi\left(\frac{\ln(x) - \ln(A_m)}{\beta_c}\right) \tag{6}$$

Typical hazard and fragility curves are shown in Fig. 1, and the $G(x)$ is plotted in Fig. 2. The latter is seen to possess two convex regions and one concave region. These are closely related to whether the seismic risk is underestimated or overestimated when the number of subintervals is small, as discussed in detail in Section 2.2. In addition, plots of $G(x)$ with varying A_m and β_c are presented in Figs. 3 and 4, respectively.

$$\left(K_I = 10^{-6}, K_H = \frac{1}{\log(3)}, A_m = 0.5, \beta_r = \beta_u = 0.35\right)$$

$$\left(K_I = 10^{-6}, K_H = \frac{1}{\log(3)}, \beta_r = \beta_u = 0.35\right)$$

$$\left(K_I = 10^{-6}, K_H = \frac{1}{\log(3)}, A_m = 0.5\right)$$

2.2. The effects of a small number of subintervals upon the results of seismic risk quantification

Using the $G(x)$ given in Eq. (6), the seismic risk given in Eq. (2) can be rewritten as Eq. (7):

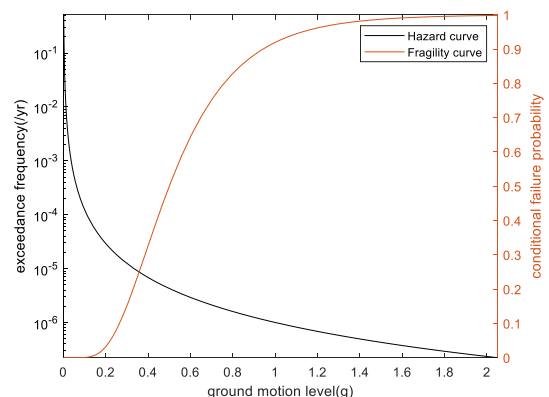


Fig. 1. Typical hazard and fragility curves.

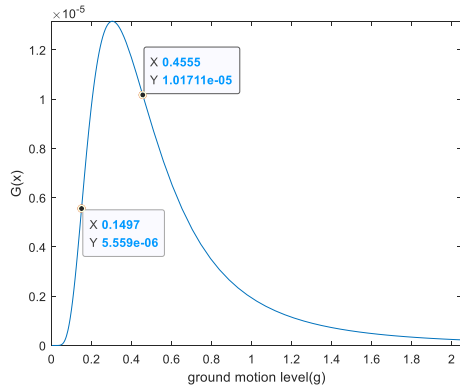


Fig. 2. The integrand ($G(x)$) of the typical hazard and fragility curves shown in Fig. 1.

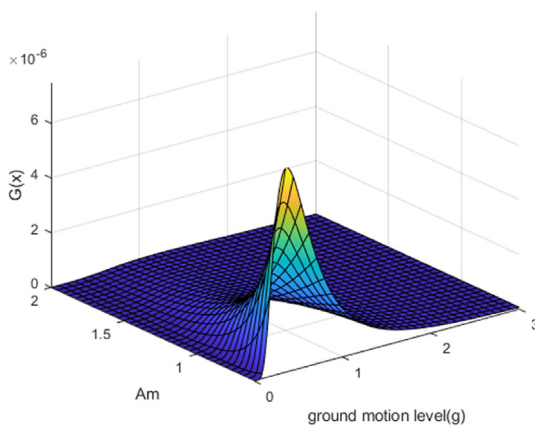


Fig. 3. The integrand ($G(x)$) of the hazard and fragility curves depending on A_m .

$$P \approx \sum_{i=1}^N G\left(a + \frac{(2i-1)}{2} \Delta x\right) \Delta x = \sum_{i=1}^N G\left(a + \frac{(2i-1)(b-a)}{2N}\right) \frac{(b-a)}{N} \tag{7}$$

When the ground motion level interval is discretized into 2^n and 2^{n+1} subintervals, the seismic risk is given as Eqns. (8) and (9), respectively:

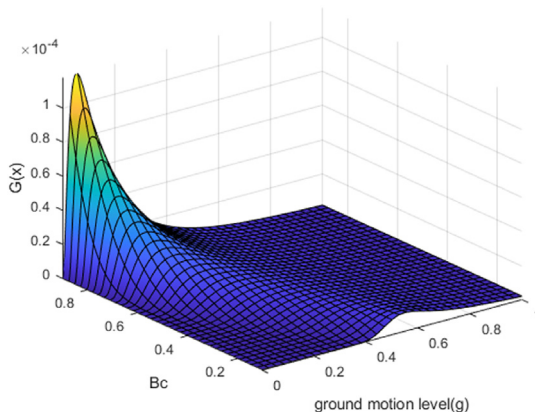


Fig. 4. The integrand ($G(x)$) of the hazard and fragility curves depending on β_c .

$$P_1 = \sum_{i=1}^{2^n} G\left(a + \frac{(2i-1)(b-a)}{2^{n+1}}\right) \frac{(b-a)}{2^n} \tag{8}$$

$$P_2 = \sum_{j=1}^{2^{n+1}} G\left(a + \frac{(2j-1)(b-a)}{2^{n+2}}\right) \frac{(b-a)}{2^{n+1}} \tag{9}$$

To facilitate a comparison of Eqns. (8) and (9), Eq. (9) is written as Eq. (10):

$$P_2 = \sum_{i=1}^{2^n} \left[G\left(a + \frac{(2(2i-1)-1)(b-a)}{2^{n+2}}\right) + G\left(a + \frac{(2(2i-1)(b-a)}{2^{n+2}}\right) \right] \frac{(b-a)}{2^{n+1}} \tag{10}$$

As shown in Fig. 2, $G(x)$ has two convex regions and one concave region. For the convex regions, the definition of the midpoint-convex [19] satisfies Eq. (11), i.e. the value of the function at the midpoint is not greater than the average of its values at the endpoints:

$$\sum_{i=1}^{2^n} \frac{1}{2} \left(G\left(a + \frac{(2(2i-1)-1)(b-a)}{2^{n+2}}\right) + G\left(a + \frac{(2(2i-1)(b-a)}{2^{n+2}}\right) \right) \frac{(b-a)}{2^{n+1}} > \sum_{i=1}^{2^n} G\left(\frac{1}{2} \left(a + \frac{(2(2i-1)-1)(b-a)}{2^{n+2}} + a + \frac{(2(2i-1)(b-a)}{2^{n+2}} \right) \right) \frac{(b-a)}{2^{n+1}} \tag{11}$$

Multiplying both sides of Eq. (11) by 2 generates the simplified Eq. (12):

$$P_2 = \sum_{i=1}^{2^n} \left(G\left(a + \frac{(2(2i-1)-1)(b-a)}{2^{n+2}}\right) + G\left(a + \frac{(2(2i-1)(b-a)}{2^{n+2}}\right) \right) \frac{(b-a)}{2^{n+1}} > \sum_{i=1}^{2^n} G\left(a + \frac{(2i-1)(b-a)}{2^{n+1}}\right) \frac{(b-a)}{2^n} = P_1 \tag{12}$$

The right-hand term of Eq. (12) is equal to P_1 in Eq. (8), i.e., the seismic risk when the ground motion level interval is discretized into 2^n subintervals. The left-hand term of Eq. (12) is equal to P_2 in Eq. (10), i.e., the seismic risk when the ground motion level interval is discretized into 2^{n+1} subintervals. This means that the seismic risk with 2^{n+1} subintervals is always greater than the seismic risk with 2^n subintervals. This indicates that the seismic risk is underestimated when using a smaller number of subintervals in the convex regions.

Similarly, it can be shown that the seismic risk is overestimated when using a small number of subintervals in the concave region, as shown in Eq. (13):

$$P_2 = \sum_{i=1}^{2^n} G\left(a + \frac{(2(2i-1)-1)(b-a)}{2^{n+2}}\right) + G\left(a + \frac{(2(2i-1)(b-a)}{2^{n+2}}\right) \frac{(b-a)}{2^{n+1}} < \sum_{i=1}^{2^n} G\left(a + \frac{(2i-1)(b-a)}{2^{n+1}}\right) \frac{(b-a)}{2^n} = P_1 \tag{13}$$

In the seismic PSA community, it has been generally believed that a small number of subintervals results in a conservative seismic risk quantification. However, Eqns. (12) and (13) show that this is only true in the concave region, not in the convex regions. Hence, a method is provided for identifying the boundaries between overestimation and underestimation of seismic risk when using a small number of subintervals in Section 3.

3. Boundaries between underestimation and overestimation

When using a small number of subintervals, the analysis in Section 2 indicated that the seismic risk, i.e., the integral of $G(x)$, can be overestimated in the convex regions, and underestimated in the concave region. The boundaries between the convex and concave regions of $G(x)$ are the inflection points, which can be obtained by using Eq. (14):

$$\begin{aligned}
 G''(x) = & (K_H + 2)(K_H + 1)K_H K_I x^{-K_H - 3} \frac{1}{2} \left(1 + \operatorname{erf} \left(\frac{\ln(x) - \ln(A_m)}{\sqrt{2} \beta_c} \right) \right) \\
 & - (K_H + 1)K_H K_I x^{-K_H - 2} \frac{1}{x \beta_c \sqrt{2\pi}} \exp \left(-\frac{(\ln(x) - \ln(A_m))^2}{2\beta_c^2} \right) \\
 & - (K_H + 1)K_H K_I x^{-K_H - 2} \frac{1}{x \beta_c \sqrt{2\pi}} \exp \left(-\frac{(\ln(x) - \ln(A_m))^2}{2\beta_c^2} \right) \\
 & - K_H K_I x^{-K_H - 1} \frac{1}{x^2 \beta_c \sqrt{2\pi}} \left(1 + \frac{\ln(x) - \ln(A_m)}{\beta_c^2} \right) \\
 & \exp \left(-\frac{(\ln(x) - \ln(A_m))^2}{2\beta_c^2} \right)
 \end{aligned} \tag{14}$$

By introducing the factor t , Eq. (14) can be simplified to give Eq. (15):

$$g(t) = C_1(1 + \operatorname{erf}(t)) - (C_2 + \sqrt{2}t) \exp(-t^2) \tag{15}$$

where:

$$t = \frac{\ln(x) - \ln(A_m)}{\sqrt{2} \beta_c}$$

$$\operatorname{erf}(t) = \int_0^t e^{-x^2} dx$$

$$C_1 = \beta_c^2 \sqrt{2\pi} (K_H + 2)(K_H + 1) \frac{1}{2}$$

$$C_2 = 2\beta_c K_H + 3\beta_c$$

Because Eq. (15) is a continuous and differentiable function, it can be solved by using numerical methods such as the Newton Raphson method [20]. However, while the Newton Raphson method provides rapid convergence, an appropriate solution may not be found with a poor initial value. Therefore, it is important to determine appropriate initial values.

The value of $G(x)$ at the midpoint of the i -th subinterval ($i = 1, \dots, N$) is given by Eq. (16):

$$G_{\text{mid},i} = G\left(\frac{x_{i-1} + x_i}{2}\right) = G\left(a + \frac{2i-1}{2} \Delta x\right) \tag{16}$$

In the convex and concave regions, Eqns. (17) and (18) hold, respectively:

$$\frac{G(x_{i-1}) + G(x_i)}{2} > G\left(\frac{x_{i-1} + x_i}{2}\right) \tag{17}$$

$$\frac{G(x_{i-1}) + G(x_i)}{2} < G\left(\frac{x_{i-1} + x_i}{2}\right) \tag{18}$$

By examining the values of $G(x_i)$ ($i = 0, \dots, N$), it is possible to identify the subintervals in which the inequality changes from Eq. (17) to Eq. (18), and vice versa. Since the values of x_i are located near the inflection points, they can be used as initial values to find the boundaries between the regions of underestimation and overestimation via the Newton Raphson method by finding the roots of $g(t) = 0$. First, the given value of x_i must be converted into t_0 using the relation in Eq. (19):

$$t_0 = \frac{\ln(x_i) - \ln(A_m)}{\sqrt{2} \beta_c} \tag{19}$$

The Newton Raphson method is a numerical method for obtaining the roots of an equation by using a tangent line and x-axis. Starting from the t_0 given in Eq. (19), iteration continues with Eq. (20):

$$t_{n+1} = t_n - \frac{g(t_n)}{g'(t_n)} \tag{20}$$

until t_{n+1} sufficiently converges to the root of the equation $g(t) = 0$.

A flowchart for identifying the boundaries between underestimation and overestimation via the Newton Raphson method is presented in Fig. 5. First, inputs such as those for the hazard data (K_I, K_H), the fragility data (A_m, β_r, β_u), and the ground motion level interval are prepared, along with the end conditions such as the error limit and the maximum number of iterations. After dividing the ground motion level into N subintervals, the initial values of x_i are obtained by examining the values of $G(x_i)$ and converting them to t_0 values. The blue part of Fig. 5 shows the procedure for finding the initial values, while the green part shows the application of the Newton Raphson method to obtain the numerical solutions of the equation $g(t) = 0$. As $g'(t_n)$ is used in Eq. (20), its value should not be zero; hence, it is necessary to avoid t_c given in Eq. (21):

$$t_c = \pm \sqrt{\frac{C_2^2 \sqrt{2\pi} - 8C_1 + 4\sqrt{2\pi}}{8\sqrt{2\pi}} - \frac{\sqrt{2}C_2}{4}} \tag{21}$$

If t_n is not equal to t_c , iterations using Eq. (20) may proceed until $t_{n+1} - t_n$ is less than a specified error limit, or until a specified maximum number of iterations is exceeded.

If $t_{\alpha,1}$ and $t_{\alpha,2}$ are found as the two roots of $g(t) = 0$, they need to be converted to ground motion levels $x_{\alpha,1}$ and $x_{\alpha,2}$ as given by Eq. (22):

$$x_{\alpha,j} = A_m \exp\left(\sqrt{2} \beta_c t_{\alpha,j}\right) \tag{22}$$

These ground motion levels are the boundaries between the regions of overestimation and underestimation when using a small number of subintervals.

4. Example

In this section, an example is considered for the hazard curve ($H(x)$) with $K_I = 10^{-6}$, $K_H = \frac{1}{\log(3)}$ and the fragility curve ($F(x)$) with $A_m = 0.5g$, $\beta_r = \beta_u = 0.35$ shown in Fig. 1, and the corresponding integrand ($G(x)$) in Eq. (1), which is shown in Fig. 2. The variables in the example are set to properly represent the usual range of those

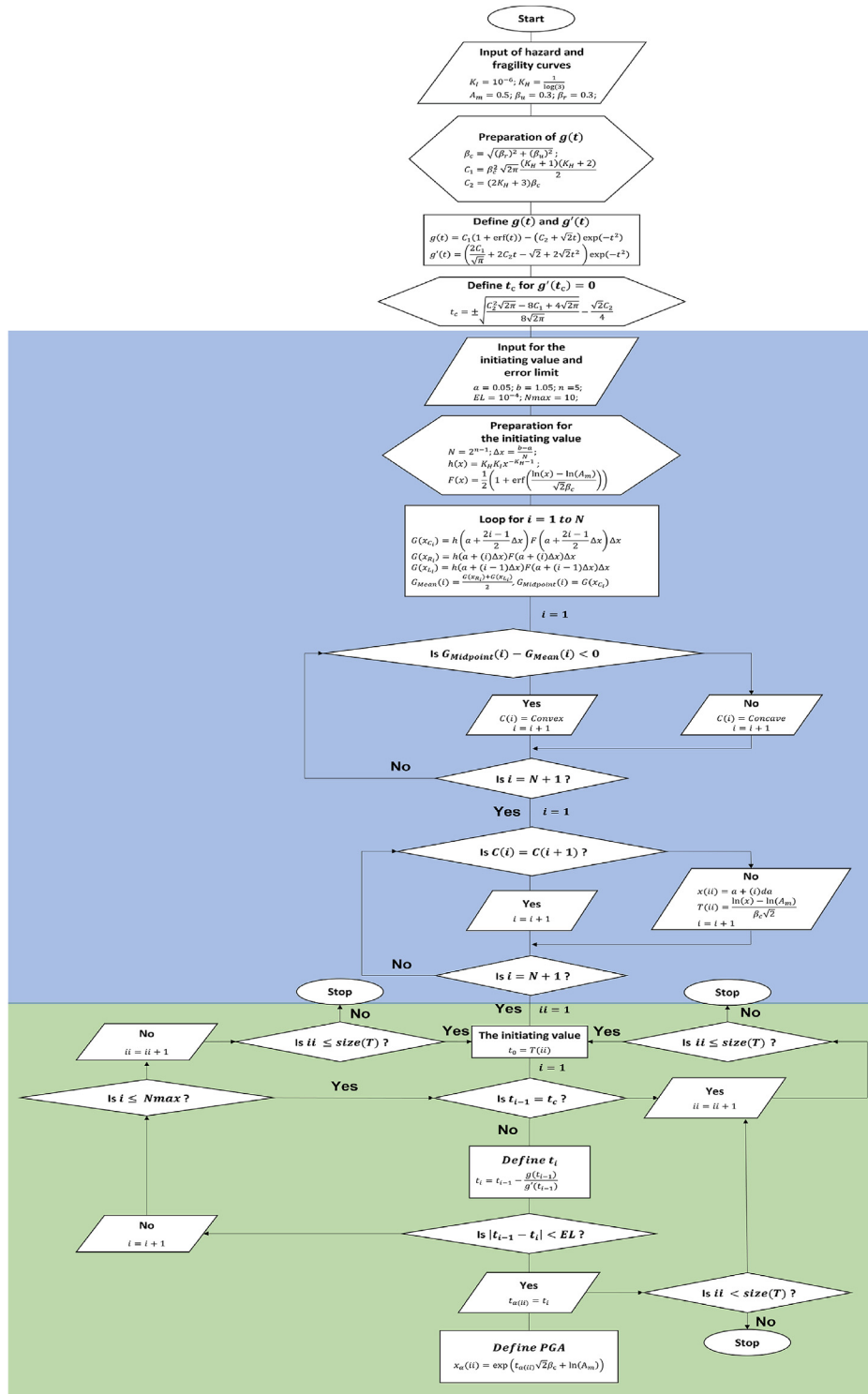


Fig. 5. A flowchart for finding the boundaries between the regions of overestimation and underestimation.

variables. Here, the ground motion level interval is from 0.05 to 1.05 g, and is evenly divided into 2^4 subintervals. From the numerical values of $G(x_i)$, the subintervals in which the inequality changes from Eq. (17) to Eq. (18) and vice versa are found to be that from 0.1125 to 0.1750 g, and that from 0.4250 to 0.4875 g, respectively. The midpoint values of these two subintervals are selected as the initial values, and the Newton Raphson method is applied to

obtain the overestimation and underestimation boundaries as 0.1497 and 0.4555 g, respectively. In the ground motion level ranges of 0–0.1497 g and 0.4555–1.05 g, $G(x)$ is convex and, hence a small number of subintervals will result in an underestimation of the seismic risk. However, in the ground motion level range of 0.1497–0.4555 g, $G(x)$ is concave and, hence, a small number of subintervals will result in an overestimation of the seismic risk. In

all regions, the seismic risk estimation approaches the correct value as the number of subintervals increases. When the number of subintervals (N) for each region is varied as 2^{n-1} ($n = 1, 2, \dots, 10$), the calculated seismic risks (Eq. (7)) in the two convex underestimation regions are as shown in Fig. 6, and those in the overestimation region are as shown in Fig. 7.

The sum of the seismic risks over all three regions obtained while varying the right-hand endpoint of the ground motion level interval (b) is shown in Fig. 8, and that obtained while varying A_m is shown in Fig. 9. The overestimation or underestimation of seismic risk when a small number of subintervals are used mainly depends on where the overestimation and underestimation regions exist in the ground motion level interval for seismic risk quantification. The right-hand endpoint (b) determines the ground motion level interval, and the location of the overestimation and underestimation regions is largely affected by the median (A_m) of the fragility curve. Therefore, A_m and b are considered to be two most important variables in determining whether the seismic risk is overestimated or underestimated when a small number of subintervals are used for seismic risk quantification. In Figs. 8 and 9, the four b 's (0.55, 1.05, 1.55, and 2.05) and the two A_m 's (0.2 and 0.6) are selected to properly demonstrate the overestimation and underestimation of seismic risk when a small number of subintervals are used.

Here, each of the three regions is discretized into 2^{n-1} ($n = 1, 2, \dots, 10$) subintervals, and the seismic risk quantification is clearly affected by the contributions from the underestimation and overestimation regions. In Fig. 8, because the boundary between overestimation and underestimation is 0.4555 g, the underestimation region widens as the ground motion level interval widens, while the overestimation region remains unchanged. Therefore, the seismic risk contribution from the underestimation region increases and, hence, it becomes more likely that the seismic risk is underestimated when using a small number of subintervals for each region. Fig. 8 demonstrates that the seismic risk is overestimated with a small number of subintervals when $b = 0.55$ and 1.05 , and underestimated when $b = 1.55$ and 2.05 . Fig. 9 demonstrates that the seismic risk is underestimated with a small number of subintervals when $A_m = 0.2$ and overestimated when $A_m = 0.6$.

From Eq. (22), the boundaries between underestimation and overestimation ($x_{\alpha,1}$ and $x_{\alpha,2}$) are proportional to A_m , and so is the overestimation region, which lies between them, as indicated by Eq. (23):

$$\Delta x_{\alpha,i} = |x_{\alpha,1} - x_{\alpha,2}| = |A_m (\exp(\sqrt{2} \beta_c t_{\alpha,1}) - \exp(\sqrt{2} \beta_c t_{\alpha,2}))| \tag{23}$$

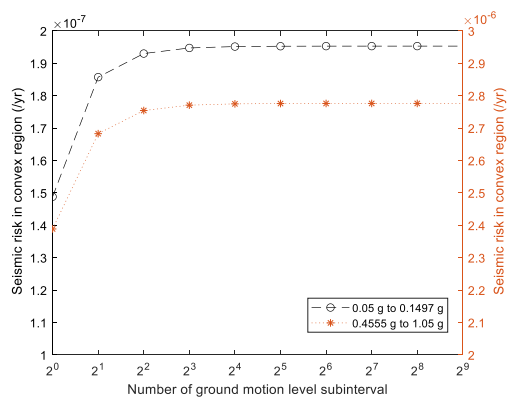


Fig. 6. The calculated seismic risk in the two convex underestimation regions as a function of the number of subintervals.

The function $G(x)$, and the boundaries ($x_{\alpha,1}$ and $x_{\alpha,2}$), for various A_m values are shown in Fig. 10. Here, the boundaries are seen to increase as A_m increases; hence, the overestimation region shifts to the right. As a result, the seismic risk tends to be overestimated when using a small number of subintervals, as shown in Fig. 9.

The seismic risk quantification results when the ground motion level interval is discretized into $1, 2^1, 2^2, \dots, 2^9$ subintervals while varying the right-hand endpoint (b) and the median capacity (A_m) are indicated in Figs. 11 and 12, respectively. Unlike Figs. 8 and 9, the seismic risks in Figs. 11 and 12 are quantified without consideration of the boundaries of the three regions (underestimation and overestimation) and hence, this approach is closer to the current practice of quantifying the seismic risk. Because $G(x)$ has two boundaries between underestimation and overestimation, the seismic risk quantification result with a small number of subintervals is heavily affected by the locations of these boundaries. Thus, in Figs. 8 and 9 above, a continuous increase or decrease in the quantified seismic risk was observed as the number of subintervals increased, whereas Figs. 11 and 12 each show an initial increase in seismic risk, followed by a decrease when the number of subintervals is small. As the right-hand endpoint of the ground motion level interval (b) increases, or A_m decreases, the underestimation region gets wider and, hence, the risk contribution from the underestimation region increases. Consequently, the seismic risk may be underestimated when the number of subintervals is small (e.g. one or two), as can be seen when $b = 1.55$ and $b = 2.05$. However, as the number of subintervals increases, the seismic risk tends to be overestimated while gradually converging to the exact value. Conversely, when the right-hand endpoint of the ground motion level interval (b) decreases, or A_m increases, the risk contribution from the overestimation region increases and, hence, the seismic risk tends to be overestimated.

5. Discussion

The discretization of the ground motion level interval into a small number of subintervals (usually around or less than five subintervals) has been widely used in seismic risk quantification to reduce the quantification burden, with the assumption that a small number of subintervals leads to a conservative quantification result. In the present study, however, a mathematical analysis has demonstrated that the seismic risk can be underestimated in some regions when using a small number of subintervals. Indeed, the effect of a small number of subintervals upon the results of seismic risk quantification is complicated, especially when the ground motion

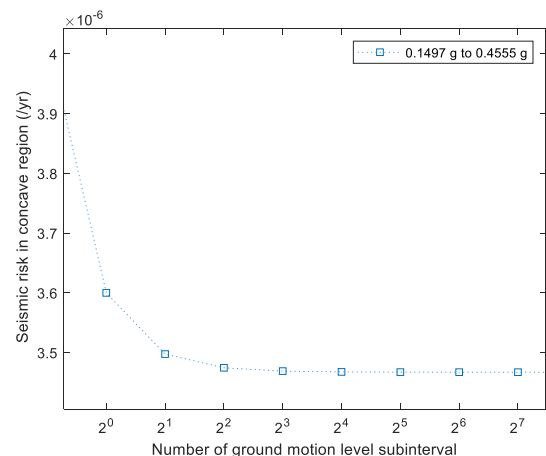


Fig. 7. The calculated seismic risk in the concave overestimation region as a function of the number of subintervals.

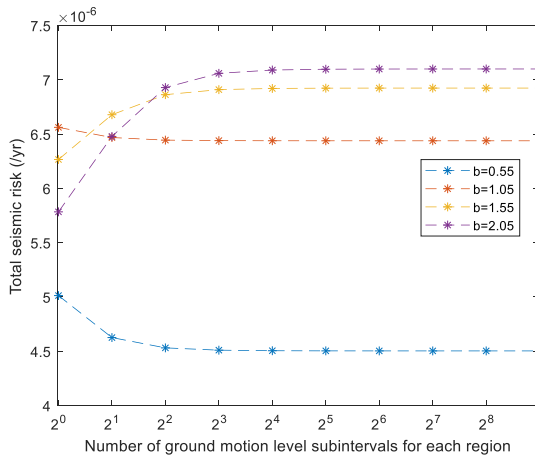


Fig. 8. The calculated seismic risk while varying the right-hand endpoint of the ground motion level interval.

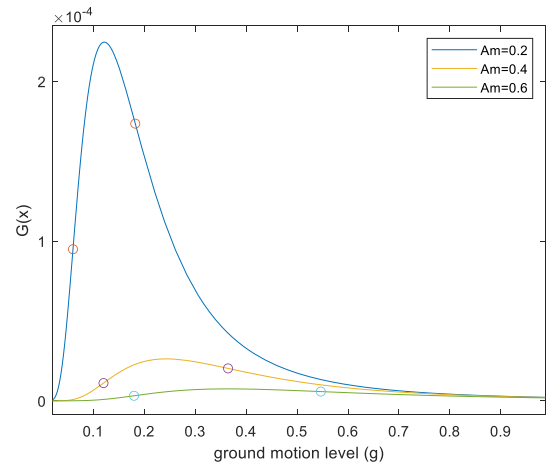


Fig. 10. The boundaries between underestimation and overestimation while varying A_m .

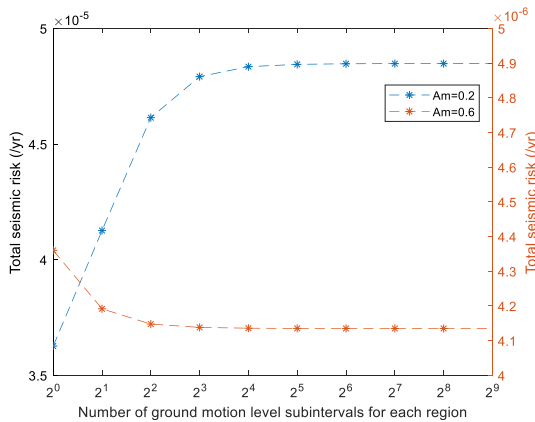


Fig. 9. The calculated seismic risk as a function of the number of subintervals while varying A_m .

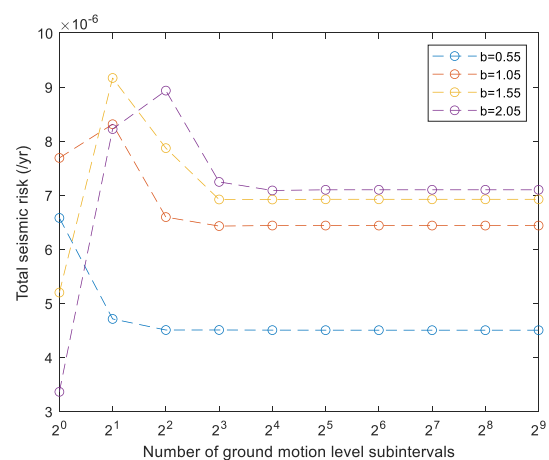


Fig. 11. The seismic risk for the ground motion level interval while varying b .

level interval is discretized without consideration of the boundaries between underestimation and overestimation. If the median capacity (A_m) is significantly smaller, or significantly larger, than the ground motion level interval, then the seismic risk may be underestimated when using a small number of ground motion level intervals. In such cases, it is likely that the analyzed ground motion level interval is dominated by the convex region of the hazard and fragility convolution curve. However, in practice, the risk contribution from the overestimation region is generally large and, therefore, it is likely that the seismic risk is overestimated when using a small number of ground motion level intervals. Nevertheless, conservative seismic risk quantification results are generally expected, even when the ground motion level interval is discretized into a small number of subintervals, and this widely-used assumption in seismic PSA is generally true except for certain extreme cases.

In brief, due to the lack of background information for determining the number of subintervals in seismic PSA, it has been believed that a small number of subintervals will yield a conservative seismic risk quantification result. The present study has demonstrated the possibility of seismic risk underestimation when using a small number of subintervals. Although the possibility of underestimation may not be significant in practice, it is recommended that the ground motion level interval be discretized into a sufficient number of subintervals (usually more than ten subintervals) to avoid the possible underestimation and reduce any unnecessary error in the quantification of seismic risk.

To be exact, the length of subintervals has greater impact on the seismic risk quantification results than the number of subintervals. However, when the ground motion level interval for seismic risk quantification is fixed, how many subintervals the ground motion level interval is divided into (i.e. the number of subintervals) is directed related to the length of each subinterval. In this sense, a small number of subintervals is meant to be synonymous with a large length of each subinterval in this paper.

A small number of subintervals results in less accurate seismic risk quantification result, while whether such quantification result is optimistic or conservative is determined by where the three regions of underestimation and overestimation are placed in the ground motion level interval for seismic risk quantification. Depending on whether the ground motion level interval for seismic risk quantification is dominated by underestimation or overestimation regions, the seismic risk quantification result becomes optimistic or conservative. As the number of subintervals increases, the seismic risk quantification result becomes less optimistic or less conservative, and then becomes closer to the exact result.

6. Conclusions

A closed form of the seismic risk for the specific ground motion level is difficult to derive because it is evaluated by convolution of the hazard and fragility curves. Recently, the seismic risk

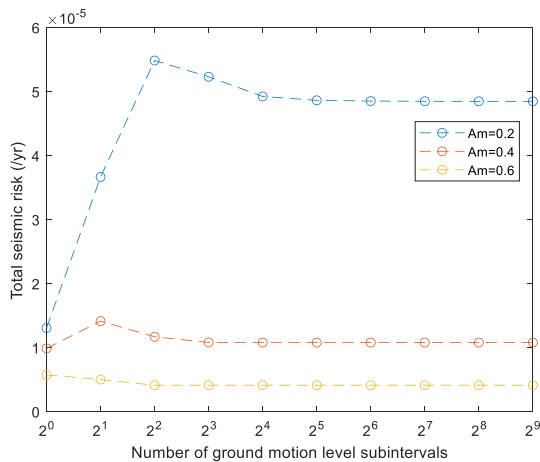


Fig. 12. The seismic risk for the ground motion level interval while varying A_m .

quantification with discretized ground motion level subintervals has become widely used. If the number of ground motion level subintervals is sufficient, the result of seismic risk quantification converges to an accurate value. However, the number of ground motion level subintervals for use in seismic PSA quantification is limited in practice. For this reason, it is necessary to understand the effects of using a small number of ground motion level subintervals upon the results of seismic risk quantification.

In the present study, the seismic risk quantification method with discretized ground motion level subintervals was analyzed to find that the quantification results can be underestimated in the convex region, and overestimated in the concave region, of the convolution of the hazard and fragility curves when using a small number of ground motion level subintervals. In view of the importance of avoiding any unintended underestimation of the seismic risk to nuclear plants, this finding is highly important to PSA analysts.

Further, the present study identified two boundaries between underestimation and overestimation, and provided a method for finding them. Moreover, the risk contribution from the overestimation region was found to be more significant than that from the underestimation regions in most practical applications. Underestimation in one region is usually compensated by overestimation in another region. Accordingly, PSA analysts must take care to avoid underestimation when quantifying the seismic risk in a specific localized region of the hazard and fragility convolution curve wherein the seismic risk can be underestimated.

In brief, the present study has revealed the possibility of underestimating seismic risk, and has provided a method for identifying the boundaries between underestimation and overestimation regions in order to assist in avoiding unintentional underestimation. This paper is expected to contribute towards widening the understanding of how the use of a small number of ground motion level subintervals affects the results of seismic risk quantification, and how to avoid any possible underestimation of the seismic risk for a nuclear power plant.

Funding

This work was supported by the Nuclear Safety Research Program of the Korea Foundation of Nuclear Safety funded by the Korean government's Nuclear Safety and Security Commission [grant number 2203027-0122-CG100, 2104028-0222-SB120].

Declaration of competing interest

The authors declare that they have no known competing financial interests or personal relationships that could have appeared to influence the work reported in this paper.

References

- [1] J. Han, A.S. Nur, M. Syifa, M. Ha, C.W. Lee, K.Y. Lee, Improvement of earthquake risk awareness and seismic literacy of Korean citizens through earthquake vulnerability map from the 2017 Pohang earthquake, South Korea, *Rem. Sens.* 13 (7) (2021) 1365.
- [2] J. Han, J. Kim, S. Park, S. Son, M. Ryu, Seismic vulnerability assessment and mapping of Gyeongju, South Korea using frequency ratio, decision tree, and random forest, *Sustainability* 12 (18) (2020) 7787.
- [3] I.K. Choi, D. Hahm, M.K. Kim, Current status and issues of external event PSA for extreme natural hazards after Fukushima accident, in: *NEA/CSNI/R(2014)*, vol. 9, 2014.
- [4] C. Seong, G. Heo, S. Baek, J.W. Yoon, M.C. Kim, Analysis of the technical status of multiunit risk assessment in nuclear power plants, *Nucl. Eng. Technol.* 50 (3) (2018) 319–326.
- [5] R.C. Kennedy, S.A. Short, *Basis for Seismic Provisions of DOE-STD-1020*. 1994, Lawrence Livermore National Lab, Brookhaven National Lab, 1994.
- [6] Electric Power Research Institute, *Seismic Probabilistic Risk Assessment Implementation Guide*, 3002000709, 2013.
- [7] B. Dasgupta, Evaluation of methods used to calculate seismic fragility curves, in: *Center for Nuclear Waste Regulatory Analyses*, 2017.
- [8] T. Zhou, M. Modarres, E.L. Drogue, An improved multi-unit nuclear plant seismic probabilistic risk assessment approach, *Reliab. Eng. Syst. Saf.* 171 (2018) 34–47.
- [9] Y. Watanabe, T. Oikawa, K. Muramatsu, Development of the DQFM method to consider the effect of correlation of component failures in seismic PSA of nuclear power plant, *Reliab. Eng. Syst. Saf.* 79 (3) (2003) 265–279.
- [10] S. Kwag, J. Park, I.K. Choi, Development of efficient complete-sampling-based seismic PSA method for nuclear power plant, *Reliab. Eng. Syst. Saf.* 197 (2020), 106824.
- [11] S. Kwag, E. Choi, S. Eem, J.G. Ha, D. Hahm, Toward improvement of sampling-based seismic probabilistic safety assessment method for nuclear facilities using composite distribution and adaptive discretization, *Reliab. Eng. Syst. Saf.* 215 (2021), 107809.
- [12] United State Nuclear Regulatory Commission, *Risk Assessment of Operational Events Handbook (Volume 2-external Events)*, 2017.
- [13] J.S. Kim, M.C. Kim, Development of a software tool for seismic probabilistic safety assessment quantification with a sufficiently large number of bins for enhanced accuracy, *Energies* 14 (6) (2021) 1677.
- [14] Electric Power Research Institute, 1020756, in: *Surry Seismic Probabilistic Risk Assessment Pilot Plant Review*, 2010.
- [15] R.P. Kennedy, Overview of methods for seismic PRA and margin analysis including recent innovations, in: *Proceedings of the OECD-NEA Workshop on Seismic Risk*, 1999.
- [16] G. Strang, *Calc.*, Vol. 1. 1991: (Wellesley Cambridge Press).
- [17] C. Scawthorn, *Earthquake Engineering*, CRC Press LLC, 1999.
- [18] R.P. Kennedy, M.K. Ravindra, Seismic fragilities for nuclear power plant risk studies, *Nucl. Eng. Des.* 79 (1) (1984) 47–68.
- [19] W.F. Donoghue, *Distributions and Fourier Transforms*, Academic Press, 1969.
- [20] K.E. Atkinson, *An Introduction to Numerical Analysis*, John Wiley & Sons Book Company, 1990.